Geometric and electronic structures of the boron-doped photocatalyst TiO_2

INSTITUTE OF PHYSICS PUBLISHING JOURNAL OF PHYSICS: CONDENSED MATTER

J. Phys.: Condens. Matter **18** (2006) 87–96 doi:10.1088/0953-8984/18/1/006

Geometric and electronic structures of the boron-doped photocatalyst TiO_2

Hua Geng[1], Shiwei Yin[1], Xia Yang[1], Zhigang Shuai[1] and Banggui Liu[2]

[1] Laboratory of Organic Solids, Institute of Chemistry, Chinese Academy of Sciences, Beijing 100080, People's Republic of China
[2] Institute of Physics, Chinese Academy of Sciences, Beijing 100080, People's Republic of China

E-mail: zgshuai@iccas.ac.cn

Received 21 July 2005, in final form 25 October 2005
Published 9 December 2005
Online at stacks.iop.org/JPhysCM/18/87

Abstract

Boron-doped anatase TiO_2 has been shown to be a much more efficient and stable photocatalyst than the pristine TiO_2. We employed the LDA-supercell approach to calculate the geometry and electronic structures of the doped systems, in order to reveal the microscopic mechanism of how photocatalytic efficiency is improved by boron doping. It is found that the boron atom tends to either replace an oxygen atom or sits in the interstitial position. It is highly unlikely for the boron atom to replace Ti. The density of states analysis shows that for oxygen-substituted doping the boron atom is strongly bonded to two oxygen atoms as well as to two Ti atoms, which results in new midgap states, and eventually the absorption edge is red-shifted and the photocatalytic efficiency is enhanced.

(Some figures in this article are in colour only in the electronic version)

1. Introduction

Since TiO_2 was found to be an efficient and stable photocatalyst more than 30 years ago [1–4], intense research efforts have been particularly devoted to the photodegrading toxic organic molecules as well as water and air purifications by TiO_2 [5–7]. The primary photochemical processes occurring upon irradiation of a semiconductor are now understood in the following way [8–10]: the photogenerated electrons and holes migrate to the surface of the semiconductor first, then these charges can either ionize the oxygen molecule or water to form chemically active radicals; eventually, these radicals can degrade the toxic molecules. In order to achieve efficient photodegradation, it is necessary for the photogenerated electron and holes to be efficiently separated and be mobile enough to reach the surfaces. Furthermore, the bandgap of the semiconductor should match the optical spectrum of solar irradiation.

The bandgap defines the wavelength sensitivity of the semiconductor to irradiation. The pristine TiO_2 is only active upon UV excitation (wavelength $\lambda < 387$ nm), whose bandgap is

3.2 eV in the anatase TiO_2 crystalline phase. Transition metal doping can expand to the responsiveness to the visible [11–18]. Recently, doping TiO_2 with non-metal atoms has received much attention [19–23]. Asahi *et al* [19] have reported progress on the nitrogen-doped TiO_2 for both powder and film samples, and they also theoretically calculated the band structure to understand how the photocatalytic efficiency is enhanced. They suggested that the oxygen sites were substituted by nitrogen atoms, and that the visible light sensitivity of the nitrogen-doped TiO_2 was due to the narrowing of the bandgap by mixing the N 2p and O 2p states. In order for the photocatalysis to be more efficient, the electron–hole pair recombination process should be suppressed. This can be accomplished by trapping the photogenerated electrons, or the photogenerated holes. As reported by Zhou *et al* [24], the nickel oxide was shown to facilitate the photoexcited electron transferring, hence the recombination of photoinduced electrons and holes can be efficiently suppressed. Very recently, Zhao *et al* [25] have improved appreciably the photocatalytic efficiency by doping TiO_2 with both non-metal boron atom and nickel oxide, Ni_2O_3. They conclude that (i) by incorporating boron atoms in the TiO_2 bulk the absorption spectrum can be extended to the visible region, and (ii) the Ni_2O_3 stays in the surface of the materials, which facilitates the electron–hole separation in the surface.

There are basically three origins for the enhanced photocatalytic efficiency by doping [19]: (i) new states within the bandgap are induced; (ii) the bottom of the conduction band, or the impurity empty states, are as high as that for the pristine TiO_2, so that its photoreduction activity is kept; (iii) the newly generated states should overlap in energy sufficiently with the continuum band states, so that the photoexcited carriers can move rapidly to the reactive sites at the catalyst surface within the lifetime.

TiO_2 doped by nonmetals, by carbon [26] or nitrogen [19, 27], has been extensively investigated by DFT calculations. Doping-induced midgap states for different doping concentrations as well as the density of states have been calculated to reveal the photocatalytic properties. In this work, we present the first-principle calculations on boron-doping-induced geometric and electronic structure modifications. The theoretical analysis provides pertinent insights to understand how the photocatalytic efficiency is enhanced in experiment [25], and eventually helps to design photocatalytic materials.

2. Methodology

The first-principle calculations were performed with a plane-wave-based pseudo-potential method within the density function theory (DFT), as implemented in the CASTEP program [28]. Exchange–correlation effects were treated with the local density approximation (LDA) [29, 30]. The core electrons were replaced by norm-conserving pseudo-potentials, with core radii of Ti, O, and B being 1.6, 1.6, and 1.4 Å respectively [31], and the valence electron configurations were $3d^2 4s^2$ for Ti atoms, $2s^2 2p^4$ for O atoms, and $2s^2 2p^1$ for B atoms. We have taken a $2 \times 2 \times 2$ supercell of 48 atoms in calculations, consisting of eight primitive cells of anatase TiO_2.

We choose 'medium' accuracy for all the calculations. It corresponds to a plane wave cut-off of 450 eV for our norm-conserving pseudopotential. It corresponds to 300 eV for ultra-soft pseudopotential as the CASTEP module within the Materials Studio package converts automatically. The total energy and the force convergence thresholds are 2×10^{-5} eV/atom and 0.05 eV $Å^{-1}$, respectively. We note that in a previous investigation of the electronic structures of Co-doped TiO_2 a plane wave cut-off is chosen as 280 eV for the ultra-soft pseudo-potential [32a], very close to our choice of cut-off. We have further tested the cut-off convergence by optimizing the pristine TiO_2 structure with increasing cut-off energies, namely, for 450, 500, 550, and 600 eV. The corresponding total energies for the primitive

cell (containing six atoms) are −1907.4823, −1907.8520, −1907.9387, and −1907.9554 eV, respectively. Namely, from 450 to 600 eV, the energy difference per atom is less than 0.08 eV. It is expected that the difference between the 450 eV cut-off and the converged one should be less than 0.1 eV/atom, because the 600 eV cut-off case already shows quite convergent behaviour. According to a general point of view, if the difference in energy per atom is less than 0.1 eV, the results can be regarded as converged [32b]. Integrations over the Brillouin zone were carried out by using the Monkhorst–Pack scheme [33] with $3 \times 3 \times 4$ k-sampling in the relevant irreducible wedge. Results have been obtained for the fully relaxed geometries including all atoms, while lattice constant are fixed.

We have considered the following three cases of doping: (i) one of the 16 Ti atoms is substituted by boron, denoted as case I hereafter; (ii) interstitial boron doping, denoted as case II; (iii) one of the 32 oxygen atoms is replaced by a boron atom, denoted as case III. For the purpose of analysing relative stability for the three cases, the following 'anion localization method' for evaluating energies is proposed: (i) subtracting one boron atom energy from and adding one Ti atom energy to the supercell energy; (ii) subtracting one boron atom energy from the supercell energy; (iii) adding one oxygen atom energy to and subtracting one boron atom energy from the supercell energy, respectively. Note that in all three cases, the boron atom energy is subtracted from the total energy. Thus, it is irrelevant to the relative stability. The Ti atom energy is obtained through calculating the Ti crystal with $p6_3/mmc$ space symmetry of within the same approach. We simply assume that the Ti atom in TiO_2 crystal possesses the same energy. Then, from the calculated total energy of pristine TiO_2, the value of oxygen atom energy can be obtained.

3. Results and discussion

The supercell structures of three cases of doping are shown in figures 1(a)–(c) for cases I, II, and III, respectively. We are mostly interested in the distorted structures around the doped boron atoms, which are displayed in figure 2 both before and after geometry optimizations. The calculated bond lengths and bond angles near the impurity atom for the three cases are presented in table 1. We found that the B atom adopts sp^3 hybridization (a B atom bonded with four O atoms) to form tetrahedral configuration for case I. From the optimized supercell structure of case II in figures 2(b2), when B is in the interstitial position, we find that there are three O atoms close to the B atom, and these four atoms form a planar structure. Therefore, the B atom in this case adopts sp^2 hybridization (a B atom bond with three O atoms). From the optimized supercell structure of case III in figures 2(c2), O being substituted by B, we note that there are two O atoms close to the B atom. The bond lengths of B–O1 and B–O2 are equal and are calculated to be 1.35 Å. In addition, there are also two Ti atoms close to the doped B atom. The distances of B–Ti1 and B–Ti2 are 2.38 and 2.37 Å, respectively, which is much shorter than the sum of the van der Waals radii for the B atom (1.55 Å) and Ti atom (1.95 Å), $1.55 + 1.95 = 3.5$ Å. This means that the Ti and B can form a covalent bond. We note that there exist both sp^3 and sp^2 hybridizations for B–O bonding in the ameghinite single crystal [34], a mineral widely existing in nature. This indicates that the B atom prefers to adopt sp^3 and sp^2 hybridizations with the neighbouring O atoms. Namely, when four O atoms are the neighbours the B atom will adopt sp^3 hybridizations, while when only three atoms are available the B atom will prefer to form sp^2 hybridizations, as is evidenced in case I and case II.

However, for case III, when B substituted the O atom before relaxation, as figure 2(c1) shows, the nearest atoms are two Ti atoms with distance of 1.93 Å. The second neighbouring atoms are two O atoms with distances 2.786 Å. In such a case, there are only two O atoms close by the B atom. The B atom is strongly bonded with the two O atoms and weakly bonded

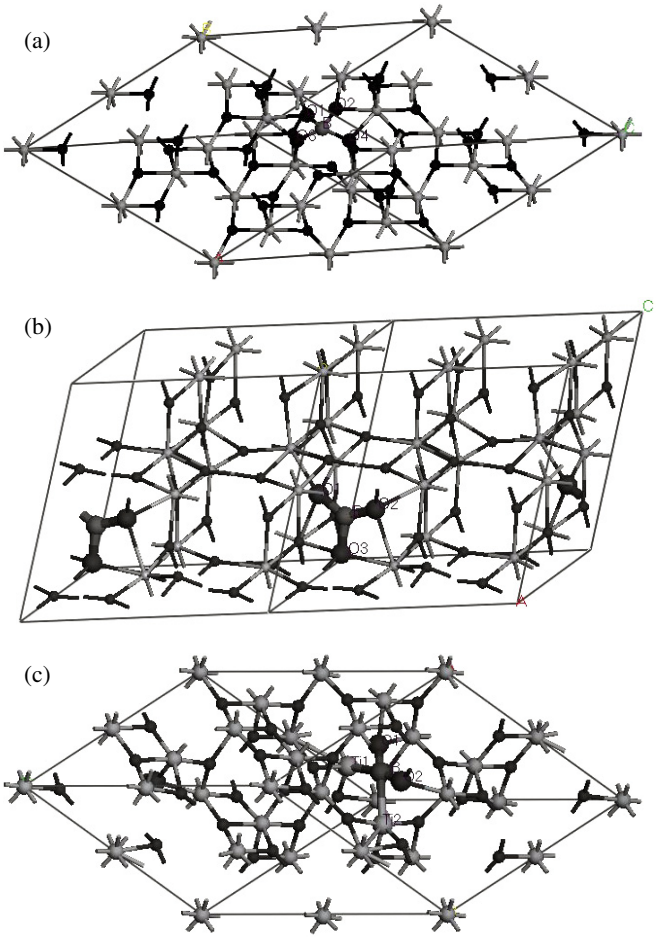

Figure 1. Supercell structures of B-doped anatase TiO_2: (a) Ti-substitution, (b) interstitial, and (c) oxygen-substitution initial and CASTEP-optimized structures.

with the two Ti atoms; see figure 2(c2). The optimized structure with comparison with the pristine one can be seen from table 1.

The DOS of pristine TiO_2 is shown in figure 3(a), which is in excellent agreement with the previous calculation by Asahi *et al* [35]. The valence band consists in mostly the O 2p orbital, the conduction band mostly the Ti 3d orbitals. It should be noted that the LDA-calculated bandgap is about 2.3 eV, while the experimental value is 3.2 eV. Namely, the theoretical bandgap accounts for 70% of the real bandgap. This is a known problem in DFT, which was pointed out in the 1970s by Kunz [36] and many others [37].

Figures 3(b) and (c) depict the calculated density of states (DOS) of doping case I and case II, in close comparison with the DOS of pristine TiO_2 (see figure 3(a)). We find that in these two systems the doped B atom does not bring appreciable modifications to the DOS near the Fermi surface. We then make a partial DOS (PDOS) analysis, which displays the contribution of the B atom to the DOS; see figures 4(a) and (b). The PDOS calculations are based on Mulliken population analysis, which considers the contribution to each energy band from a given atomic orbital. The local DOS (LDOS) is generated by adding all the contributions

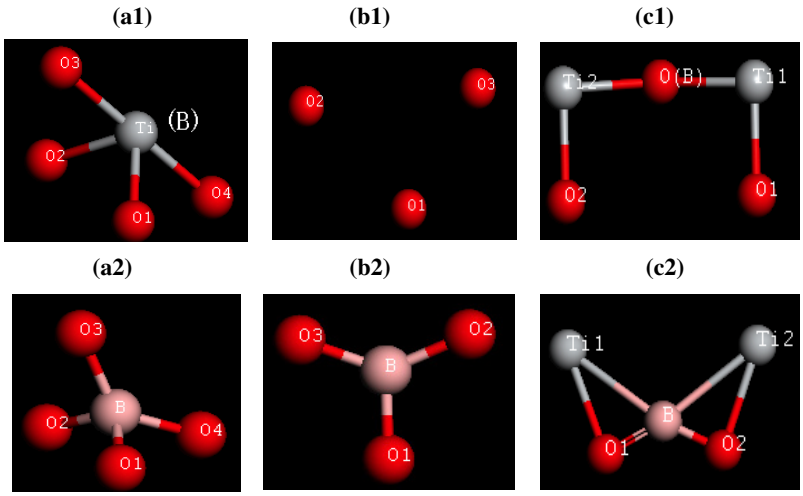

Figure 2. B impurity neighbouring structures of initial (a1) Ti substitution, (b1) interstitial, and (c1) O substitution; B impurity neighbouring structures of the CASTEP-optimized (a2) Ti substitution, (b2) interstitial, and (c2) O substitution.

Table 1. The impurity induced geometric modifications for the three cases.

Doping cases	Bond lengths/angles	Pristine structure	Optimized structure
I Ti atoms substituted by boron	B(Ti)–O1	1.93 Å	1.41 Å
	B(Ti)–O2	1.93 Å	1.408 Å
	B(Ti)–O3	1.973 Å	1.473 Å
	B(Ti)–O4	1.973 Å	1.473 Å
	B(Ti)–O5	1.930 Å	2.510 Å
	B(Ti)–O6	1.930 Å	2.512 Å
	∠O1–B(Ti)–O2	92.443°	113.034°
	∠O2–B(Ti)–O3	78.084°	93.994°
	∠O4-B(Ti)–O1	101.916°	93.915°
	∠O4–B(Ti)–O3	180.00°	131.425°
II Interstitial boron doping	O1–O2	3.057 Å	2.247 Å
	O2–O3	2.773 Å	2.237 Å
	O3–O1	3.794 Å	2.494 Å
	∠O1–O2–O3	52.7°	56.4°
	∠O2–O3–O1	46.2°	56°
	∠O3–O1–O2	81°	67.6°
III O atoms replaced by boron	B(O)–O1	1.93 Å	1.35 Å
	B(O)–O2	1.93 Å	1.35 Å
	B(O)–Ti1	1.93 Å	2.38 Å
	B(O)–Ti2	1.93 Å	2.37 Å
	∠Ti1–O1–B(O)	92.44°	85.5°
	∠B(O)–O2–Ti2	92.44°	84.6°
	∠O1–B(O)–O2	85.3°	128.2°

together from the atomic orbitals on a given atom. We found that the p electronic states of the doped B atom locate at the bottom of the valence band (−6 to −8 eV). This is related to the

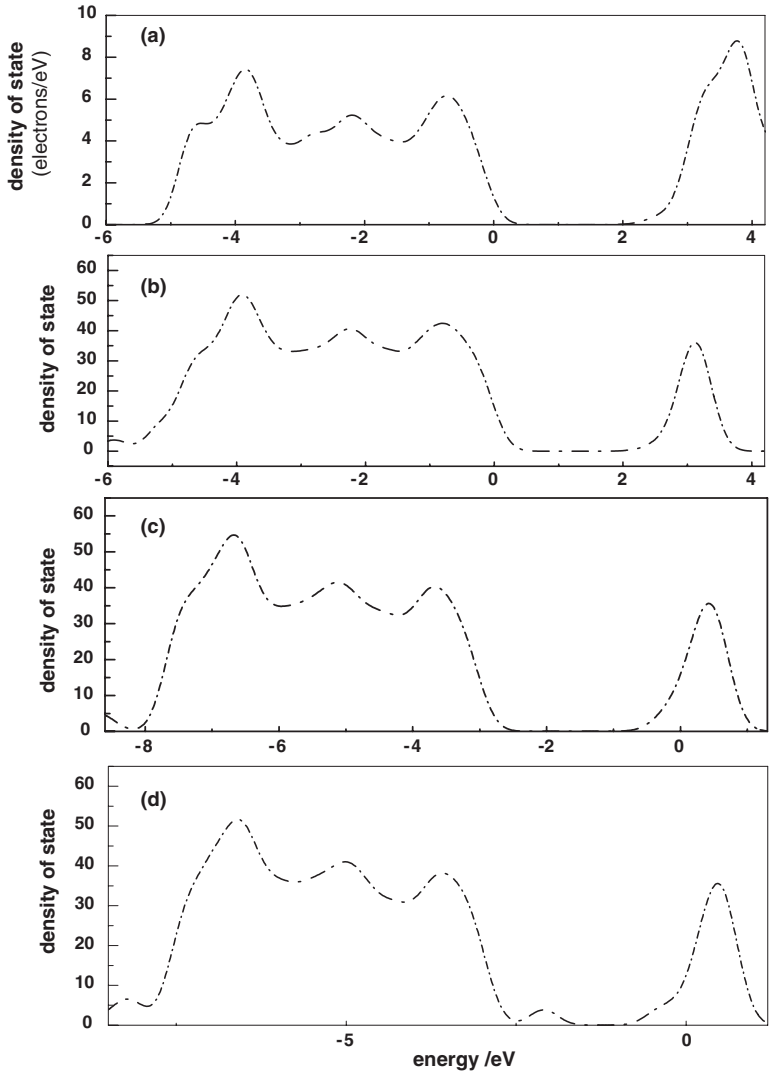

Figure 3. DOS of (a) pristine anatase TiO_2, (b) Ti substituted by B, (c) interstitial B doping, and (d) O substituted by B.

symmetric environment of the impurity: by forming stable sp^3 or sp^2 hybridization, the lattice distortion is quite localized, then the impurity would not affect the charge density beyond the second-nearest neighbour atoms. Such a kind of doping can form deep impurity levels in the energy spectrum, and the induced electronic level is buried at the bottom of the valence band. Therefore, it is expected that in these two cases the doping would not shift the absorption edge, and thus would not contribute to enhance the photocatalytic efficiency.

However, for case III, figure 4(c), the DOS projections for the B impurity atom not only contribute to the low-energy part (~ -8 eV), but also to the high-energy portion (-2 eV), close to the Fermi surface. In addition, the neighbouring Ti atoms and O atoms also contribute to form the midgap state; see figures 5(a) and (b). The lower portion forms a deep impurity

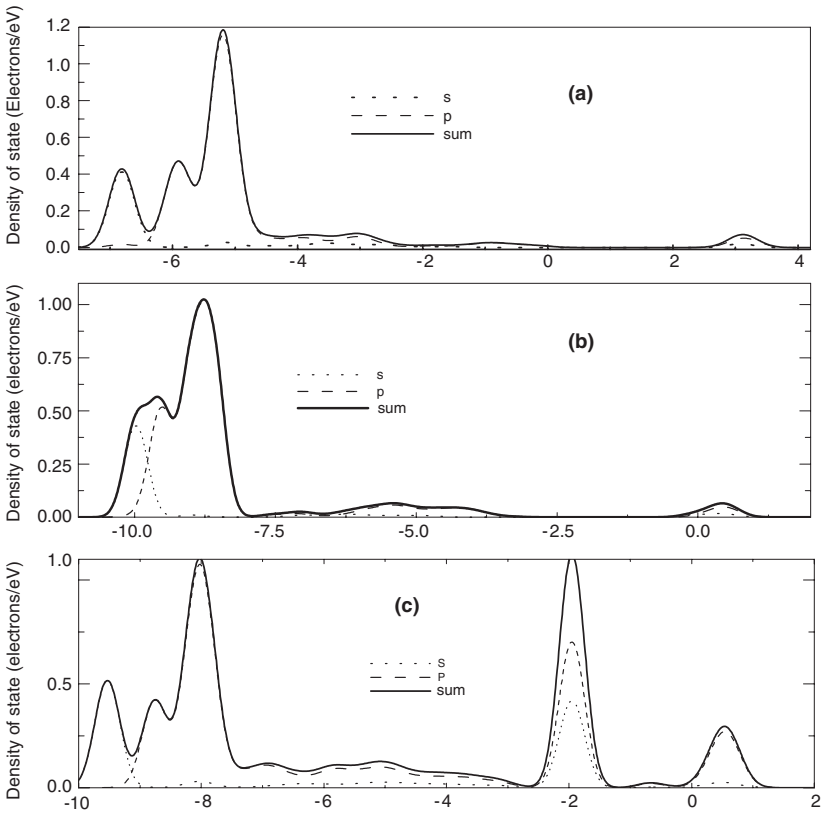

Figure 4. (a) Projected DOS for B contribution in Ti substitution; (b) projected DOS for B contribution in interstitial doping; (c) projected DOS for B in O substitution.

level at the bottom of the valence band due to the B–O strong covalent bond, as in case I and case II. The B–Ti and Ti–O weak bond will lead to a shallow energy level, so we can see that the neighbouring Ti atoms and O atoms and B atom together contribute to the midgap state. Because of the strong electro-negativity of B compared with the neighbour O atom, there appears appreciable electron transfer from B to O, and from Ti to B, so the impurity would affect the charge density of the nearest and the second-nearest, and even beyond the second-nearest neighbours. The effect of the impurity would not be localized. A qualitative rationalization for the relative positions of the B impurity bands can be understood as follows. The impurity is located in an asymmetric environment, with strong electronegative O atoms on one side, and a less electronegative impurity species on the other. The B atom loses some of its charge to the neighbouring O atoms, and thus becomes somewhat positively charged; that is to say, the B becomes effectively ionized. The second-nearest Ti atom will lose some of its charge to the B atom; therefore, the binding energy of this substitution will be smaller than cases I and II.

That the impurity state is delocalized can be seen from the DOS of the crystal with O substituted by B doping (figure 3(d)). It overlaps with the top of the valence band, i.e., the 2p electronic state of the O atoms. Figures 4(c) and 5(a) indicate that the deep levels of the B impurity and its neighbouring O atoms locate at the same energy range (-10 to -8 eV). This means that the B impurity and its neighbouring O atoms strongly overlap. However,

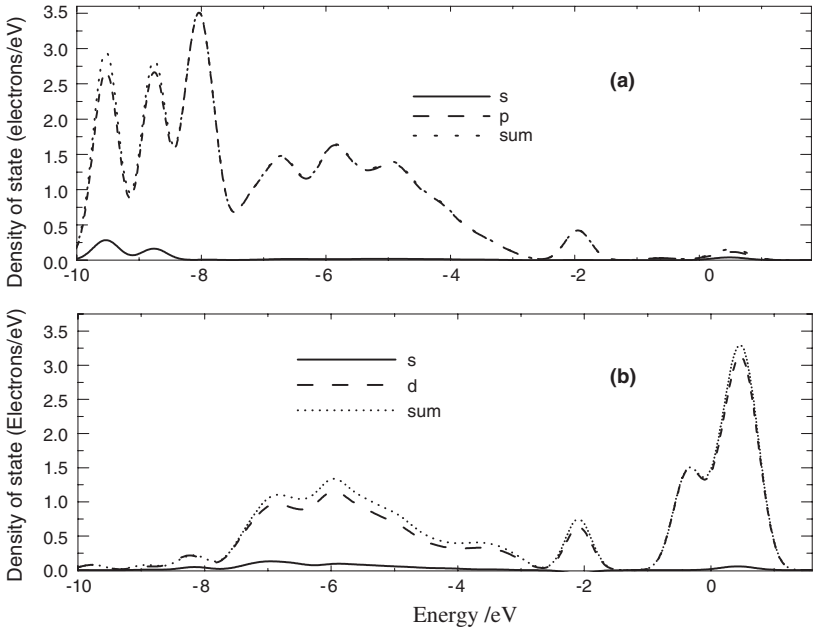

Figure 5. (a) Projected DOS for the O atoms which are closely linked to B in system III; (b) projected DOS for the Ti atoms neighbouring the impurity B atom.

from figure 5(b), there is no contribution from the Ti atom in the same energy range. This implies that Ti and B have very weak interaction, which further confirm our analysis based on electronegativities.

If we look at the valence band at ~ -2 eV, the B impurity together with its neighbouring O atoms and Ti atoms contribute to the impurity-related midgap states at the top of the valence band, which means that there exist weak B–Ti as well as Ti–O interactions. It should be noted that in the DOS calculations for the supercell we have kept only a few empty bands as in the pristine case to reduce the computational efforts: by and large, doping effects are revealed by the modifications near the top of the valence band and the bottom of the conduction band.

Finally, we make a comparison on the total energies for the three doping cases in order to reveal their relative structural stabilities. The total energies are calculated according to the schemes described in section 2, and are found to be $-15\,332.5$, $-15\,338.2$, and $-15\,337.3$ eV for the three cases, respectively. We can find that case I (the Ti substituted B doping system) is the most unstable one. However, as to systems II and III, their stability energies are quite close to each other. If we subtract the energy of a B atom in a B single crystal with space group 166 $R\bar{3}m$, then the total energies become $-15\,255.09$, $-15\,260.77$, and $-15\,259.87$ eV, respectively[3]. In another word, the relative energy for II and III is about 0.11 eV per unit cell, with interstitial doping slightly lower in energy than the O-substituted situation. Such a small difference is beyond the accuracy of the present approach. Both cases II and III can occur in the real materials, and the O-substitution is responsible for the red-shift of absorption edge.

[3] These values are slightly different from the previous results as reported in the supporting materials of [25]. In this work, a full geometry optimization has been carried out for all the systems, while in [25] only single point energies are considered.

4. Conclusion

Through first-principle DFT-LDA calculations, we have carefully examined three different doping mechanisms. We show that a B atom can be doped into TiO_2 either in the interstitial position or at the O site: their energy difference is not substantial. The O substitution will lead to narrowing of the bandgap. The induced impurity states overlap sufficiently with the 2p electronic states of oxygen. Furthermore, in the conduction band, the boron-induced state is not located in the band edge, so that the photoexcited electron can be as mobile as in the pristine materials. Both satisfy the conditions for achieving highly efficient photocatalytic function, which we believe are responsible for the experiment of Zhao *et al* [25].

Acknowledgments

The authors are indebted to Professor Jincai Zhao and Dr Wei Zhao for discussions. This work is supported by National Science Foundation of China (grant Nos 10425420, 90301001, 20420150034, 20421101). The numerical calculations are carried out in the CNIC Supercomputer Center of the Chinese Academy of Sciences.

References

[1] Fujishima A and Honda K 1972 *Nature* **238** 37
[2] Hadjiivanov K I and Klissurski D K 1996 *Chem. Soc. Rev.* **25** 61
[3] Heller A 1995 *Acc. Chem. Res.* **28** 503
[4] Linsebigler A, Lu G and Yates J T 1995 *Chem. Rev.* **95** 735
[5] Fox M A 1983 *Acc. Chem. Res.* **16** 314
[6] Hoffmann M R *et al* 1995 *Chem. Rev.* **95** 69
[7] Ollis D F and Al-Ekabi H (ed) 1993 *Photocatalytic Purification and Treatment of Water and Air* (Amsterdam: Elsevier)
[8] Bard A J 1979 *J. Phys. Chem.* **83** 3146
[9] Bard A J 1979 *J. Photochem.* **10** 150
[10] Bard A J 1980 *Science* **207** 139
[11] Ghosh A K and Maruska H P 1997 *J. Electrochem. Soc.* **124** 1568
[12] Maruska H P and Ghosh A K 1979 *Sol. Energy Mater.* **1** 237
[13] Matsumoto Y, Kurimoto J, Amagasaki Y and Sato E 1980 *J. Electrochem. Soc.* **127** 2148
Matsumoto Y, Kurimoto J, Amagasaki Y and Sato E 1981 *J. Electrochem. Soc.* **128** 1040
[14] Goodenough J B 1980 *Adv. Chem. Ser.* **186** 113
[15] Salvador J B 1980 *Adv. Chem. Ser.* **12** 413
[16] Lam R U E, DeHaar L G J, Wiersma A W, Blasse G, Tinnemans A h a and Macker A 1981 *Mater. Res. Bull.* **16** 1593
[17] Wong W K and Malati M A 1986 *Sol. Energy* **36** 163
[18] Kutty T R N and Avudaithai K 1989 *Chem. Phys. Lett.* **163** 93
[19] Asahi R, Morikawa T, Ohwaki T, Aoki K and Taga Y 2001 *Science* **293** 269
[20] Khan S U M, Al-Shahry M and Ingler W B Jr 2002 *Science* **297** 2243
[21a] Sakthivel S and Kisch H 2003 *Angew. Chem. Int. Edn* **42** 4908
[21b] Sakthivel S and Kisch H 2003 *Chem. Phys. Chem.* **4** 487
[22a] Burda C, Lou Y, Chen X, Samia A C S, Stout J and Gole J l 2003 *Nano Lett.* **3** 1049
[22b] Umebayashi T, Yamaki T, Tanaka S and Asai K 2003 *Chem. Lett.* **32** 330
[22c] Irie H, Washizuka S, Yoshino N and Hashimoto K 2003 *Chem. Commun.* 1298
[23a] Irie H, Watanabe Y and Hashimoto K 2003 *J. Phys. Chem.* B **107** 5483
[23b] Gole J L, Stout J D, Burda C, Lou Y and Chen X 2004 *J. Phys. Chem.* B **108** 1230
[23c] Lindgren T, Mwabora J M, Avendano E, Jonsson J, Hoel A, Granqvist C and Lindquist S 2003 *J. Phys. Chem.* B **107** 5709
[24] Zou Z G, Ye J H, Sayama K and Arakawa H 2001 *Naure* **414** 625
[25] Zhao W, Ma W, Chen C, Zhao J and Shuai Z 2004 *J. Am. Chem. Soc.* **126** 4782

[26] Wang H and Lewis J P 2005 *J. Phys.: Condens. Matter* **17** L209–13
[27] Di Valentin C, Pacchioni G and Selloni A 2004 *Phys. Rev.* B **70** 085116
[28] Umebayashi T, Yamaki T, Itoh H and Asai K 2002 *Appl. Phys. Lett.* **81** 454
[29] Segall M D, Lindan P L D, Probert M J, Pickard C J, Hasnip P J, Clark S J and Payne M C 2002 *J. Phys.: Condens. Matter* **14** 2717
[30] Ceperley D M and Alder B J 1980 *Phys. Rev. Lett.* **45** 566
[31] Hamann D R, Schluter M and Chiang C 1979 *Phys. Rev. Lett.* **43** 1494–7
[32a] Weng H, Yang X, Dong J, Mizuseki H, Kawasaki M and Kawazoe Y 2004 *Phys. Rev.* B **69** 125219
[32b] Lee M H, Lin J S, Payne M C, Heine V, Milman V and Crampin S 2005 *Psi-k Newslett.* **67** 145
[33] Monkhorst H J and Pack J D 1976 *Phys. Rev.* B **13** 5188
[34] Dal N A, Pozas J M M and Ungaretti L 1975 *Am. Mineral.* **60** 879
[35] Asahi R, Taga Y, Mannstadt W and Freeman A J 2000 *Phys. Rev.* B **61** 7459
[36] Kunz A B 1972 *Phys. Rev.* B **6** 606
[37] Sham L J and Schluter M 1985 *Phys. Rev.* B **32** 3883
Sham L J and Schluter M 1983 *Phys. Rev. Lett.* **51** 1888
Perdew J P 1986 *Int. J. Quantum Chem. Symp.* **19** 497
Perdew J P and Levy M 1983 *Phys. Rev. Lett.* **51** 1884